Simulation Analysis of the Collision of Lithium Battery Packages under Railway Shunting Conditions

Yuzhao ZHANG, Yulu DENG, Qianwei YIN, Jianqiang WANG

***Abstract*—To enhance the safety protection design of power lithium battery packaging in railway transportation, this paper investigates the mechanical response of lithium battery packaging components under different collision modes and thermal-mechanical coupling conditions during railway shunting operations. By establishing a railway vehicle shunting collision model and a thermal-mechanical coupling model of lithium batteries, numerical simulations were conducted to analyze the effects of coupling speeds on impact force, acceleration, and thermal stress under three collision modes: multi-vehicle-to-multi-vehicle, single-vehicle-to-multi-vehicle, and multi-vehicle-to-single-vehicle. The results indicate that increasing the coupling speed raises the impact force, but the multi-vehicle-to-multi-vehicle mode generates significantly lower impact forces compared to the other modes at the same speed. In single-vehicle-to-multi-vehicle and multi-vehicle-to-single-vehicle modes, the hook force between colliding vehicles is much larger than that of non-colliding vehicles, while this difference is negligible in the multi-vehicle-to-multi-vehicle mode. The study further determines the packaging performance and safe speed thresholds for different impact modes. Additionally, under high-temperature conditions, thermal stress distribution decreases from the exterior to the interior of the battery, with maximum stress observed at contact points with cushioning rubber pads. This research provides theoretical guidance for the design and operational protocols of lithium battery packaging in railway shunting operations.**

***Index Terms*—Lithium battery transport, Battery impact, Mechanical response, Vehicle impact, Computer simulation**

NOMENCLATURE

C_p	the equivalent specific heat capacity
ρ	the equivalent density
λ_x	the thermal conductivity along the x direction
λ_y	the thermal conductivity along the y direction
λ_z	the thermal conductivity along the z direction
$C_{p,i}$	the specific heat capacity of different structural materials of lithium batteries
ρ_i	the density of different structural materials of lithium batteries
V_i	the volume of different structural materials of lithium batteries
q_d	the convective heat transfer quantity
h	the convective heat transfer coefficient
T_∞	the ambient temperature
T_s	the surface temperature of the battery
A	the surface area of the battery
P	the surface feature length
f_1 , n	the correction coefficient
ε_{ij}	total stress
ε_{ij}^{me}	the mechanical strain
ε_{ij}^{T}	the thermal strain
E	Young's modulus
ν	Poisson's ratio
σ	stress,
α	the coefficient of thermal expansion
δ_{ij}	the Dirac function
σ_{ij}^{D}	the bias stress tensor
m_i	the mass of the vehicle
x_i	the displacement of the cushioning device
$\dot{x}_i$	the velocity of the cushioning device
$\ddot{x}_i$	the acceleration of the cushioning device
$F_i(\Delta x_i, \Delta \dot{x}_i)$	the force from the cushioning device
R_i	the vehicle motion resistance
v_i	the vehicle speed,
r_{vi}	the vehicle motion resistance ratio
g	gravitational acceleration
c	the hook buffer damping
k_s	the hook buffer stiffness
k_c	the vehicle body stiffness.
m	the mass of the lithium battery package
F	the external force

Manuscript received December 17,2024; revised April 12, 2025.

This work was supported in part by the Joint Scientific Research Fund of Gansu Province under Grant no. 24JRRA851, the Scientific and Technological Research and Development Program Project of China National Railway Group Company Ltd. Under Grant no. N2023S022, 2023F006-A(JB).

Yuzhao Zhang is a Professor of the School of Traffic and Transportation, Lanzhou Jiaotong University, Lanzhou 730070, China (e-mail: zhangyuzhao-81@mail.lzjtu.cn).

Yulu Deng is a postgraduate of the School of Traffic and Transportation, Lanzhou Jiaotong University, Lanzhou 730070, China (Corresponding author, phone: +86 17352150006, e-mail: 3257615849@qq. com).

Qianwei Yin is a postgraduate of the School of Traffic and Transportation, Lanzhou Jiaotong University, Lanzhou 730070, China (e-mail: yinqianwei2721@163.com).

Jianqiang Wang is a Professor of the School of Traffic and Transportation, Lanzhou Jiaotong University, Lanzhou 730070, China (e-mail: xinxiwjq@126.com).

I. Introduction

POWER lithium batteries are widely used in energy storage systems, electric vehicles , and portable devices due to their advantages of high operating voltage, high specific energy, and no pollution [1], and with the increase of energy density, the requirements for the safety of lithium-ion batteries are getting higher and higher[2]. The principal causes of lithium-battery deformation and failure involve mechanical abuse, electrical abuse, and thermal abuse [3]. Among them, mechanical abuse ranks as the most critical factor leading to battery failure. The temperature rise also has an impact on the mechanical properties of lithium batteries. Given that the container is closed, in a high-temperature environment during summer, due to factors like thermal radiation and heat conduction, the temperature inside the box keeps rising [4]. As a result, the volume of the lithium battery expands, and its internal stress increases. At extremely high temperatures, it can even trigger battery fracture and mechanical degradation[5]. During railroad transportation, trains often undergo grouping operations. The shunting impact conditions represent one of the most severe scenarios in railroad transportation, where vehicles are exposed to longitudinal impacts. Thus, studying the mechanical response of lithium-battery packages during shunting operations holds great practical significance.

Currently, both domestic and international researchers have conducted numerous studies on the thermal behavior and mechanical deformation of lithium-ion batteries. Chen et al. [6] simplified the three-dimensional thermal model of lithium-ion batteries and the layered structure of the battery's core region into a homogeneous material. This approach significantly enhanced computational efficiency without sacrificing accuracy. However, this study only considered the thermal behavior of lithium-ion batteries during discharge in isolation and did not account for the coupling of electrochemical factors or external forces. Nie et al. [7] designed an electrochemical-thermal coupling model. They employed equivalent density, specific heat capacity, and thermal conductivity. Although this model was highly accurate, it came with a high computational cost. Suo et al. in literature [8] established a two-way coupling model between heat and mechanics for 18650 LIBs. They analyzed the battery's discharge process by incorporating factors such as cell-surface thermal radiation, cell deformation, and temperature. This allowed them to study the temperature and stress distribution during battery discharge. Based on previous research, in literature [9], the internal heat-production rate of the battery was no longer regarded as a constant. Instead, its value was treated as a variable influenced by temperature and stress. Different factors' effects on temperature and stress were discussed, and the calculated results were compared with the experimental results from literature [7] to verify the model's accuracy. Liu et al. [10] and Yuan et al. [11] developed a mechanical multi-physics coupling model involving discharge, short-circuit, and battery temperature. Their aim was to improve battery safety under mechanical abuse conditions. Kang et al. [12] formulated a thermal analysis model for battery packs under forced convection. However, they overlooked the impact of thermal radiation on battery temperature. Notably, all the above-mentioned studies centered on the charging and discharging processes of lithium batteries. The working conditions during container transportation, where lithium batteries are inactive yet endure substantial impacts, were not explored. Gong et al. [13] probed into the mechanical response characteristics of all-paper lithium-battery transport packaging components during the drop process and validated the packaging's protective performance. Li et al. [14] designed a cushioning transportation package for lithium-ion batteries using EPP foam and corrugated boxes. Huang et al. [15] studied the SOC response characteristics of lithium-power batteries and the battery's thermal-runaway characteristics under two impact forms: plane impact and cylindrical impact. Bai et al. [16] examined the critical velocity and back-layering length of smoke propagation when a lithium-ion-battery- powered car catches fire in a tunnel. Zheng et al. [17] presented a hybrid approach that combines two meshes and domain-decomposition strategies to solve the coupled Navier-Stokes-Darcy problem. Keerthika et al. [18] put forward an improved iterative scheme based on the DGJM method for solving functional equations of a certain form $u = f + N(u)$. Nevertheless, there is a lack of research on the mechanical response of lithium batteries in relation to the specific features of railroad plane shunting. Thus, a model under such conditions requires further investigation.

Moreover, regarding the study of longitudinal inertial forces in trains, Wang [19] indicated that longitudinal inertial forces are detrimental to the longitudinal stability of cargo. Specifically, the most harmful aspect is the impact force between vehicles (or groups) during shunting operations. Wu et al. [20] created an impact test simulation model to analyze the impact scenarios in the railroad transportation of military wheeled equipment. Crăciun et al. [21] discovered that the distribution and magnitude of longitudinal forces in the train during braking are influenced by the train's length. They also analyzed the changes of these forces over time, as well as the distribution of maximum compression and tensile forces in the traction and cushioning devices. In literature [22], the effect of motion resistance on the longitudinal train force was further explored. This was done by comparing the results of two working conditions, one with and the other without the introduction of additional motion resistance. Cruceanu et al. [23] analyzed the impact of an anti-skid device on the train's longitudinal force during emergency braking while in motion. Wang et al. [24] developed a mechanical parameter-free dynamic longitudinal train force simulation model. This model simplifies the process of running the program and interpreting results, emphasizing the acceleration and deceleration values when the train is under traction or braking. Zhao [25] constructed a segmented dynamic model of friction buffers and elastic mastic buffers during the connection process and optimized these two types of buffers. Fu [26] and Wang [27] focused on the internal structure of the buffer, analyzed its impedance characteristic curve, and established the kinetic equation of the buffer. Zeng et al. [28] studied the train linkage problem on small-radius curves. Chang et al. [29] analyzed how factors such as train formation length, gradient difference, and hook gap affect the longitudinal force during the braking of extra-long heavy-duty trains on flat and straight roads. Wen et al. [30] analyzed the driving safety performance of long-formation

heavy-duty trains in long downhill curved road sections under the braking mode. Peng [31] employed both static-dynamic modeling and simulation to model and calculate the dynamic system of railroad truck loading conditions. However, these literatures only analyzed single-force situations. They did not take into account the temperature factor, which is crucial to consider simultaneously. This is because temperature affects the internal stress distribution of large lithium power batteries.

In this paper, the 1P7S power lithium-battery pack from CATL (Contemporary Amperex Technology Co., Limited) is taken as the research subject. Based on the principle of thermal coupling, the mechanical responses of the power lithium-battery's iron-box packaging components and carton -packaging components are respectively studied. The study focuses on the plane-shunting process in the railroad grouping yard during containerized railroad transportation, with an internal temperature of 73.2 ℃ [32]. The working conditions that could lead to the damage of the power lithium -battery packaging components are derived. The structure and technical route of this paper are presented in Figure 1. During the shunting operation, the external forces and environmental heat act on the vehicle model. Then, the external forces and heat transferred to the vehicle further act on the lithium battery within the container. The change in temperature causes the battery to expand, thereby influencing the stress-strain relationship. Similarly, the battery deformation affects the temperature through volumetric strain. The coupling mechanism is depicted in Figure 2. Since the lithium battery is not charged or discharged during transportation, the chemical heat generated by self-discharge is extremely small and can be disregarded. Therefore, the impact of electrochemical reactions on the thermal behavior of lithium batteries is not considered.

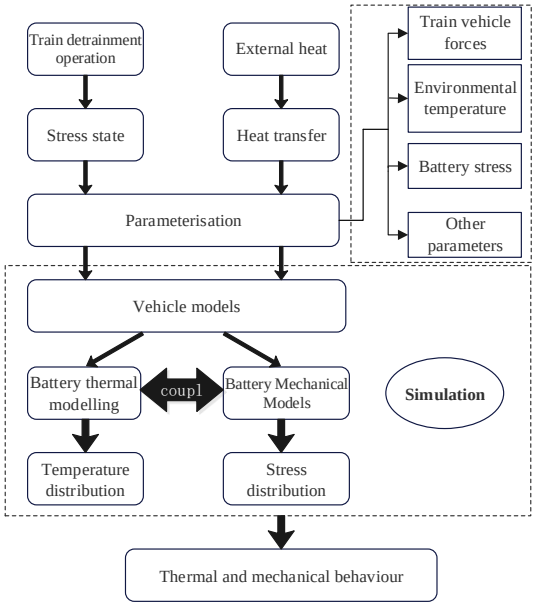

Fig. 1. Article structure and technical route.

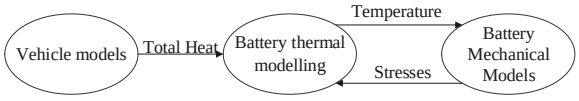

Fig. 2. Schematic diagram of environment-vehicle-cargo coupling mechanism.

II. Model Formulations

A. Thermal modeling of lithium batteries

Thermal stress arises due to temperature variations and is associated with both thermal and mechanical principles. Equations (6) and (8) elucidate the thermal-mechanical coupling mechanism of the battery. The temperature is determined through convective heat transfer between the ambient environment and the battery, as well as through thermal conduction within the battery itself. This temperature value is subsequently incorporated into the battery stress model to compute the thermal stress generated within the battery.

The energy conservation equation for the battery is:

$$\rho C_P \frac{\partial T}{\partial t} = \lambda_x \frac{\partial^2 T}{\partial x^2} + \lambda_y \frac{\partial^2 T}{\partial y^2} + \lambda_z \frac{\partial^2 T}{\partial z^2} + q_d + q_r \tag{1}$$

the equivalent specific heat capacity C_p and the equivalent density ρ are calculated by Eqs.(2) and (3), respectively; the thermal conductivity λ_x , λ_y , λ_z represent the thermal conductivity along the x , y , and z directions, respectively, which are calculated by Eqs.(4) and (5)[33], and the convective heat transfer quantity q_d is calculated by Eq. (6).

$$C_P = \frac{\sum C_{P,i} V_i}{\sum V_i} \tag{2}$$

$$\rho = \frac{\sum \rho_i V_i}{\sum V_i} \tag{3}$$

Where $C_{p,i}$ and ρ_i respectively represents the specific heat capacity and density of different structural materials of lithium batteries, V_i represents the volume, but if calculated separately, spend a lot of computational costs and improve the accuracy is very small, from the literature [6] can be seen, it is regarded as a homogeneous material can be simplified to simplify the calculations and will not affect the accuracy of the results. Therefore, it is assumed:

(1) The material inside the cell is homogeneous.

(2) The thermophysical parameters of the material are constant.

$$\lambda_x = \lambda_y = \frac{\sum \lambda_i L_i}{\sum L_i} \tag{4}$$

$$\lambda_z = \frac{\sum L_i}{\sum \frac{L_i}{\lambda_i}} \tag{5}$$

$$q_d = hA(T_\infty - T_s) \tag{6}$$

in which h is the convective heat transfer coefficient, the convective condition in the container environment is natural convection, and its value is determined by equation (7), T_∞ is the ambient temperature, T_s is the surface temperature of the battery, and A is the surface area of the battery.

$$h = f_1 \left(\frac{|T_\infty - T_s|}{P}\right)^n \tag{7}$$

where P is the surface feature length, f_1 , n is the correction coefficient [34], the values of which are shown in Table 1.

TABLE Ⅰ
COEFFICIENT VALUES USED IN EQUATION (7)

Geometry	Condition	$f_1(Wm^{n-2}K^{-n-1})$	n
Horizontal plate	Width > 0.152m, upper surface $T_s > T_a$ or lower surface $T_s < T_a$	1.36133	0.25
	Width > 0.152m, upper surface $T_s < T_a$ or lower surface $T_s > T_a$	0.680665	0.25
	Width < 0.152m, upper surface $T_s > T_a$ or lower surface $T_s < T_a$	0.830233	0.33
	Width < 0.152m, upper surface $T_s < T_a$ or lower surface $T_s > T_a$	0.415117	0.33
Vertical plate	Height > 0.152m	1.485088	0.25
	Height < 0.152m	0.941145	0.35

B. Mechanical modeling of lithium batteries

Assuming that the battery material in the Power Model is isotropic and elastic, Young's modulus and thermal expansion coefficient are both isotropic constant values. The stress ε_{ij} of the battery is the sum of the mechanical strain ε_{ij}^{me} and the thermal strain ε_{ij}^{T} caused by the temperature change., as shown in equation (8):

$$\varepsilon_{ij} = \varepsilon_{ij}^{me} + \varepsilon_{ij}^{T} = \frac{1}{E}((1+\nu)\sigma_{ij} - \nu\sigma_{kk}\delta_{jj}) + \alpha\Delta T\delta_{ij} \quad (8)$$

where E denotes Young's modulus, the value of which was experimentally derived from literature [21], ν is Poisson's ratio, σ denotes stress, α is the coefficient of thermal expansion, and δ_{ij} is the Dirac function, which takes the value of 1 when $i = j$ and 0 when $i \neq j$.

The von-Mises stress is commonly used to characterize the magnitude of thermal stresses applied to lithium batteries and is determined by equation (9):

$$\sigma_{\nu-M} = \sqrt{\frac{2}{3}\sigma_{ij}^{D}\sigma_{ij}^{D}} \quad (9)$$

where σ_{ij}^{D} denotes the bias stress tensor, determined from equation (10):

$$\sigma_{ij}^{D} = \sigma_{ij} - \frac{1}{3}\sigma_{kk}\delta_{ij} \quad (10)$$

C. Vehicle linkage crash model

The vehicle collision process can be regarded as a multi-rigid body system considering mass, elasticity and damping, with the vehicle as a rigid body connected by elastic and damping elements in the middle, and each vehicle only has degrees of freedom along the longitudinal direction of the track. The equations of motion between vehicle i and $i+1$ can be expressed by equation (11):

$$\ddot{y}_i = \frac{F_i(y_i, \dot{y}_i) - F_{i+1}(y_{i+1}, \dot{y}_{i+1}) + R_{i+1}(v(t))}{m_{i+1}} + \frac{F_i(y_i, \dot{y}_i) - F_{i-1}(y_{i-1}, \dot{y}_{i-1}) - R_i(v(t))}{m_i} \quad (11)$$

where m_i denotes the mass of the vehicle, $x_i, \dot{x}_i, \ddot{x}_i$ denote the displacement, velocity and acceleration of the cushioning device respectively, $F_i(\Delta x_i, \Delta \dot{x}_i)$ denotes the force from the cushioning device, and $\Delta x_i = x_i - x_{i+1}$ denotes the relative displacement between the cushioning devices for ease of description, $y_i = \Delta x_i$ is introduced.

The vehicle motion resistance R_i is determined by equation (12):

$$R_i = m_i \cdot g \cdot r_{vi} \cdot 10^{-3} \quad (12)$$

where v_i denotes the vehicle speed, r_{vi} denotes the vehicle motion resistance ratio, and motion resistance is a characteristic unique to each type of vehicle and is calculated using empirical equations (13) and (14):

Rolling bearing trucks:

$$r_{vi} = 0.92 + 0.0048v + 0.000125v^2 \quad (13)$$

Slide bearing trucks:

$$r_{vi} = 1.07 + 0.0011v + 0.000236v^2 \quad (14)$$

The hitch buffer can be regarded as a spring damping system and its force is calculated by equation (15):

$$F_i(y_i, \dot{y}_i) = m_i \ddot{x}_i + c\dot{x}_i + k_s x_i + k_c x_i \quad (15)$$

where c is the hook buffer damping, k_s is the hook buffer stiffness, and k_c is the vehicle body stiffness.

Finally, according to Newton's second law, the force on the cargo inside the vehicle is calculated by Eq. (16) in the process of vehicle collision:

$$F = m\ddot{x}_i \quad (16)$$

Where m is the mass of the lithium battery package and F is the external force.

In the equations mentioned above, the thermal-coupling model is composed of Eqs. (8)-(10). In this model, the mechanical strain is calculated in the following way. Based on Eqs. (11)-(16), the external force exerted on the lithium-power battery during the connection process can be solved. Then, using solid mechanics principles, the stress state of the battery can be derived. Eqs. (2)-(7) are used to calculate the temperature change. This change in temperature is incorporated into the first term on the right-hand side of Eq. (8). As a result, it has an impact on the total strain of the battery.

III. NUMERICAL SIMULATION AND RELATED PARAMETERS

A. Calculation of vehicle collision processes

In this paper, four X70 container-specific flat cars (assigned numbers 1, 2, 3, and 4 respectively) are chosen. This type of vehicle is equipped with an MT-2 hook buffer and uses 20ft standard railroad containers as carriers. Three different impact modes are established:

1. Multi-vehicle-to-multi-vehicle impact: Multiple moving lorry vehicles collide with multiple stationary cargo vehicles. For example, moving vehicles 1 and 2 impact stationary vehicles 3 and 4.

2. Single-vehicle-to-multi-vehicle impact: A moving lorry vehicle collides with multiple stationary cargo vehicles. For instance, moving vehicle 1 impacts stationary vehicles 2, 3, and 4.

3.Multi-vehicle-to-single-vehicle impact: Multiple moving lorry vehicle collides with a stationary cargo vehicles. For instance, moving vehicle 2,3,4 impacts stationary vehicles 1.

The vehicle-collision linkage process is explored through the MATLAB numerical simulation method. The specific parameters are presented in Table 2:

TABLE Ⅱ
NUMERICAL SIMULATION PARAMETERS

parameters	Symbol	value
Vehicle quality	m_i	83.36t
Maximum travel of hook buffer	Δx_i	83mm
Hook buffer stiffness	k_s	$10^6 N/m$
Hook buffer damping	c	8900Ns/m
Body stiffness	k_c	$10^6 N/m$
gravitational acceleration	g	$9.81 m/s^2$

B. Power lithium battery thermal coupling simulation

Iron box packaging

In this paper, the 1P7S model Li-ion ternary battery pack from CATL is chosen as the research target. The dimensions of the battery pack are 1.4192m×1.019m×0.2117m. Inside the container, the Li-ion battery is rigidly fixed, meaning it has no freedom of movement in the x, y and z directions. Its outer packaging consists of a 5-mm-thick iron box, with six cushioning rubbers placed inside, as depicted in Fig. 3(a). The simulation software Comsol Multiphysics 6.2 is employed for analysis. Initially, the geometric model of the lithium-power battery is constructed. Subsequently, relevant parameters are set to complete the pre-processing stage and generate the mesh.

The parameters include three parts: (1) battery pack geometric parameters, including material composition, size, etc.; (2) thermal parameters, including specific heat capacity, density, thermal conductivity, thermal expansion coefficient, etc.; and (3) mechanical parameters, including Young's modulus, Poisson's ratio, etc. The thermal and mechanical parameters of the battery materials are shown in Table 3:

Corrugated Box Packaging

The carton is fabricated using 7 mm thick BC corrugated cardboard. Although corrugated cardboard is inherently a nonlinear material, in accordance with the dynamic calculation requirements of Comsol Multiphysics, it can be defined as an isotropic material. For the calculation, the modulus of elasticity is taken as its average value. The geometric model of the corrugated-cardboard-packed structure is depicted in Fig. 4 (a), and the meshing of this model is shown in Fig. 4 (b). The attribute table of the corrugated cardboard is obtained from the relevant information presented in Table 4.

TABLE IV
MATERIAL PARAMETERS OF CORRUGATED BOARD

Parametric	Unit	value
Young's modulus	MPa	500
Poisson's ratio	—	0.35
Densities	kg/m^3	317

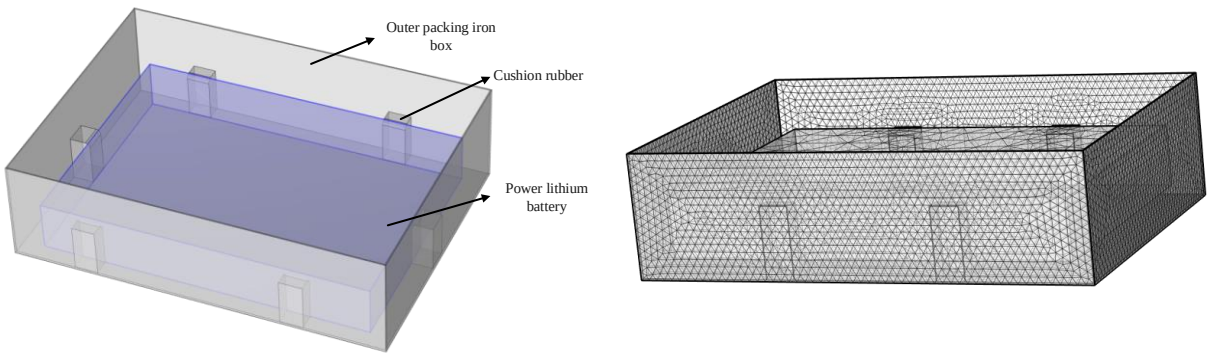

(a) (b)

Fig. 3. Geometric modeling and meshing of iron box packaging parts: (a) Geometric modeling of battery packs; (b)Thermodynamic model meshing.

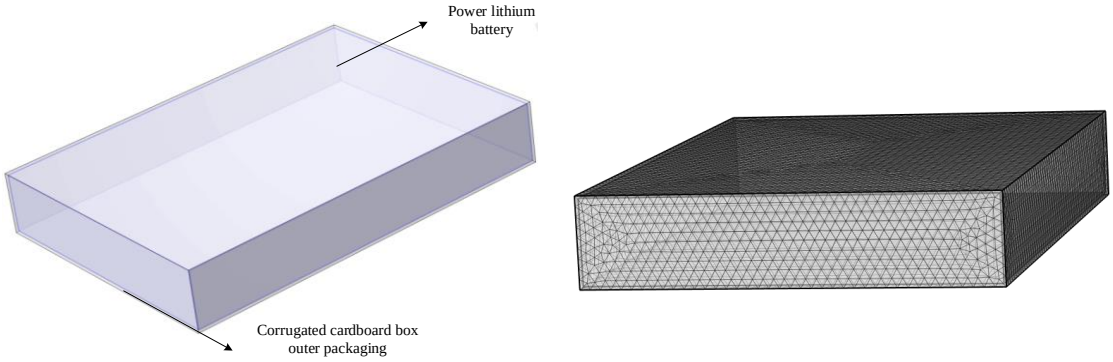

(a) (b)

Fig. 4. Geometric model and meshing of corrugated carton packaging parts:(a) Geometric modeling of battery packs; (b)Thermodynamic model meshing.

TABLE III
THERMAL AND MECHANICAL PARAMETERS OF BATTERY MATERIALS

Parametric	Unit	Outer packing iron box	Cushion rubber	battery body
Young's modulus	GPa	206	6×10^{-3}	0.07954
Poisson's ratio	—	0.25	0.47	0.3
Thermal conductivity	$W/m/K$	45	0.5	$\lambda_{x,z}=29.048$ $\lambda_y=1.1282$
Specific heat capacity	$J/kg/K$	448	1900	1329.8
Densities	kg/m^3	7872	1190	1123.8
Coefficient of thermal expansion	$1/K$	11.7×10^{-6}	2×10^{-4}	4.6×10^{-6}

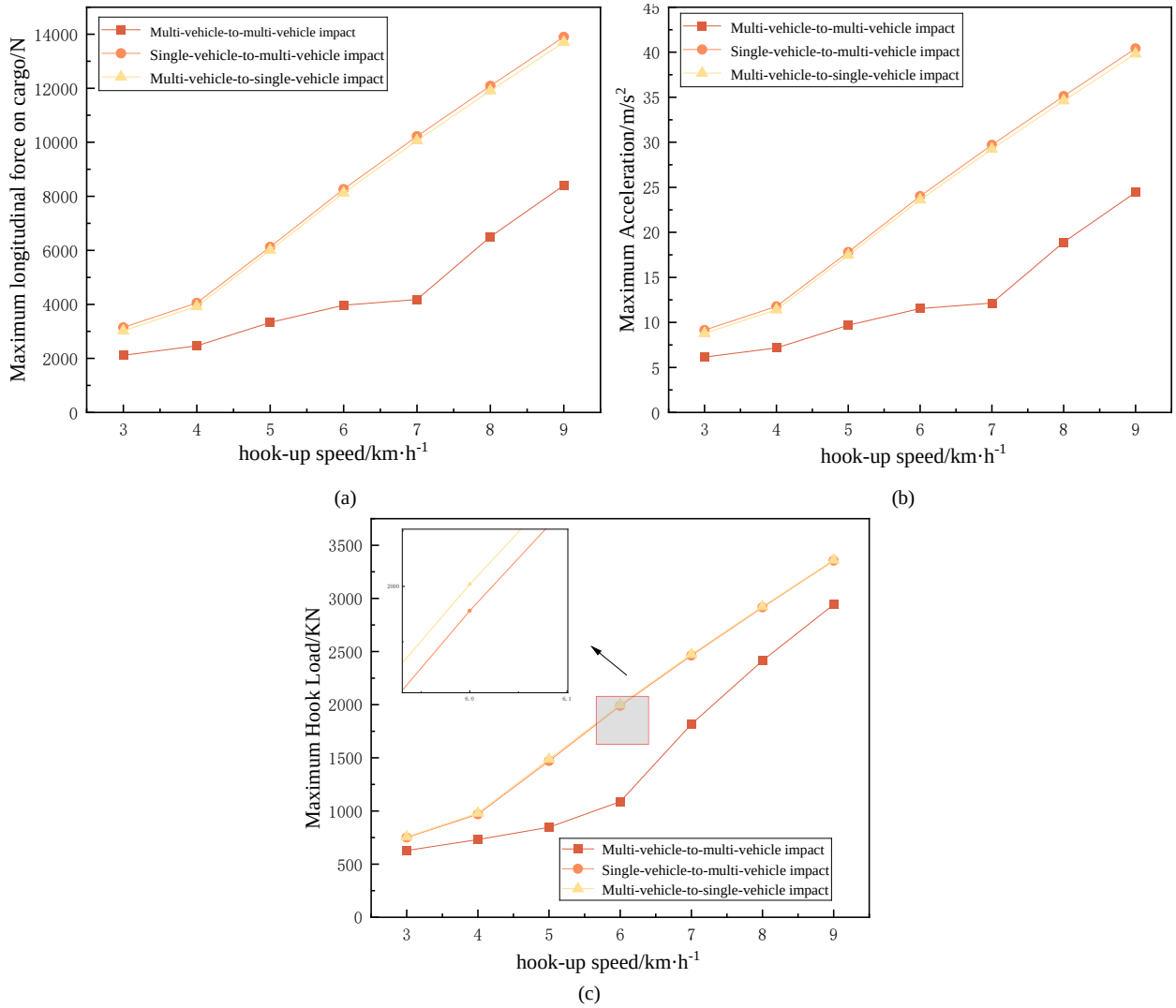

Fig. 5. Change curve of cargo force under different impact modes: (a) Maximum longitudinal force on cargo with different impact modes; (b) Maximum longitudinal acceleration of cargo in different impact modes; (c) Maximum hook load in different impact modes.

IV. NUMERICAL RESULTS AND DISCUSSION

In accordance with China's 'Railway Technical Management Regulations', the shunting speed of wagons at grouping stations should not exceed 5 km/h. In this part of the numerical analysis, this speed is regarded as a critical point. The subsequent findings also indicate that the average shunting speed can satisfy the safety requirements. By means of simulation, the stress and temperature distribution of the lithium-battery under shunting conditions is computed. Additionally, the impacts of different parameters on temperature and stress are investigated.

A. Influence of impact modes on cargo forces

This subsection examines the influence of different impact modes during various shunting processes on the forces acting on the lithium-power battery inside the freight train, specifically the initial condition of the second term on the right-hand side of Eq. (8). Given the complexity and variety of field conditions, the actual coupling speed can be greater than, less than, or equal to the safe coupling speed. Figure 4 depicts the longitudinal inertia force, longitudinal acceleration, and the maximum load on the cargo hook under different impact modes and at different speeds. It is evident that regardless of the impact type, a higher coupling impact is similar and more significant than that in the multi-

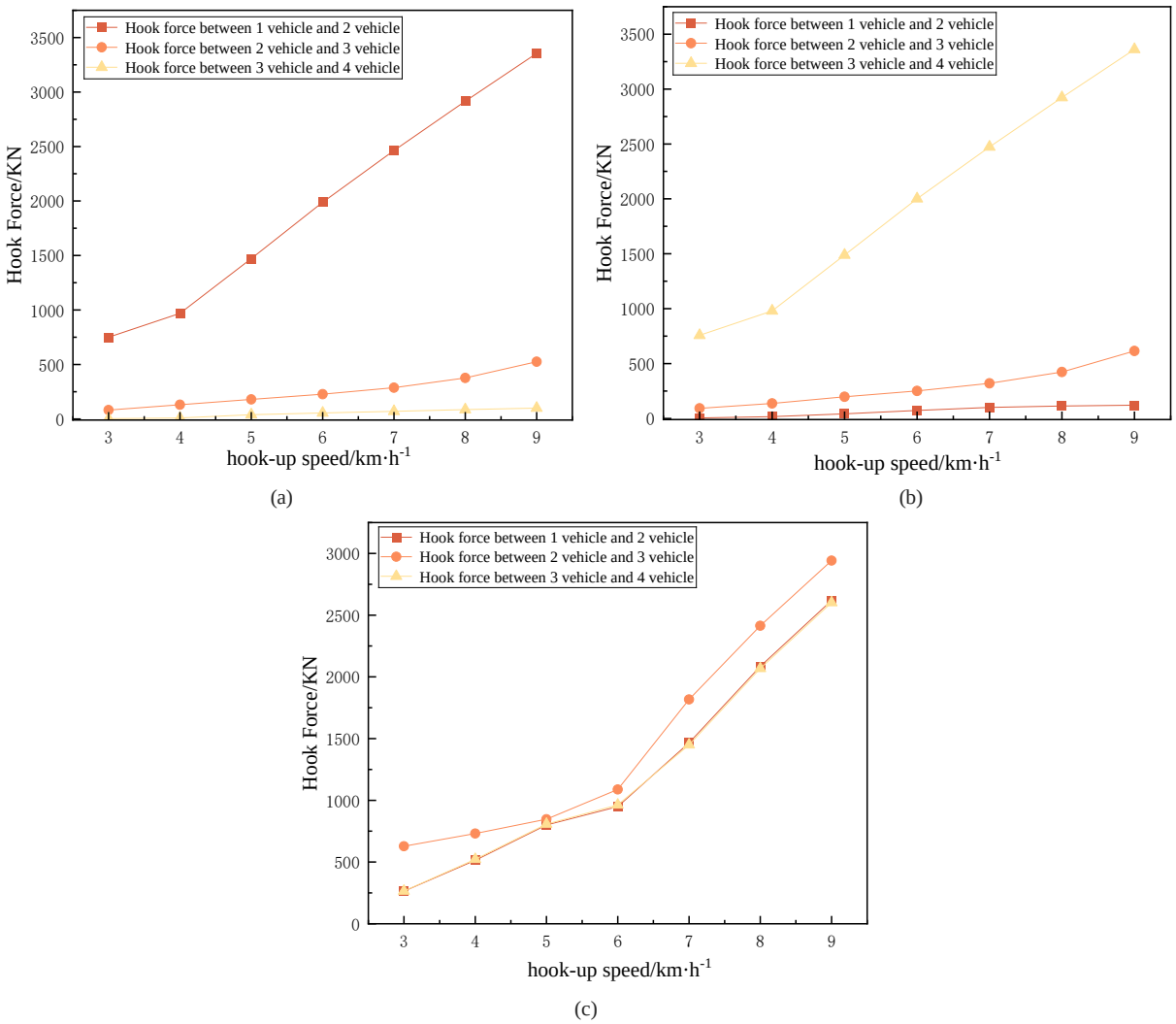

Fig. 6. Influence curve of shunting operation program on cargo forces: (a) Hook forces at different positions in single-vehicle-to-multi-vehicle impact;(b) Hook forces at different positions in multi-vehicle-to-single-vehicle impact; (c) Hook force at different positions in multi-vehicle-to-multi-vehicle impact

vehicle-to-multi-vehicle impact mode. This gives rise to the result presented in Fig. 5(a): the maximum longitudinal force on the cargo in the single-vehicle-to-multi-vehicle impact and the multi-vehicle-to-single-vehicle impact is similar and more substantial than that in the multi-vehicle-to-multi-vehicle impact mode. This is because, during the collision in the first two modes, due to the conservation of momentum, the common velocity after the collision is shown in Eq. (17).

$$v' = \frac{m_1}{m_1 + m_2} v_1 \tag{17}$$

In the formula, m_1 represents the total mass of the impacted vehicle group with a velocity of v_1, m_2 denotes the mass of the impacting vehicle group, and v' is the common velocity after the collision. The difference in mass and velocity between the impacting and impacted vehicles is more pronounced, the resulting impulse is more significant, leading to a larger hook load within the same collision time, as illustrated in Fig. 5(c), and consequently, a greater longitudinal inertia force and acceleration. Conversely, in the multi-vehicle-to-multi-vehicle impact mode, due to the similar mass of the impacting and impacted vehicles, the impulse generated is smaller than that in the previous two modes, resulting in smaller longitudinal inertia forces and accelerations. In the multi-vehicle-to-multi-vehicle impact mode, when the coupling speed exceeds 7 km/h, the maximum longitudinal force of the load increases sharply. This is because, at this point, the hook buffer reaches its maximum compression stroke, and the buffer fails. The residual energy cannot be absorbed and is directly exerted on the car body. In conclusion, during the operation process, efforts should be made to ensure that the vehicle is coupled within the safe speed range and to adopt the multi-vehicle-to-multi-vehicle coupling mode. This helps to reduce the impact on the goods during the vehicle-coupling process and prevent damage to the goods.

B. Impact of shunting operations program on cargo forces

This subsection delves into the impact of shunting operation scenarios during different shunting processes on the forces acting on the internal power lithium-battery of a freight train. Once again, this pertains to the initial condition of the second term on the right-hand side of Eq. (8). Fig. 6 shows the forces on the cargo at different train positions for various impact modes. In the multi-vehicle-to-multi-vehicle impact mode, the difference between the hook force of two neighboring wagons and the hook force of the two wagons in collision is relatively small. However, in the single-vehicle-to-multi-vehicle and multi-vehicle-to-single-vehicle impact modes, the hook force of the two wagons in collision is significantly larger than that of the other two wagons. This is

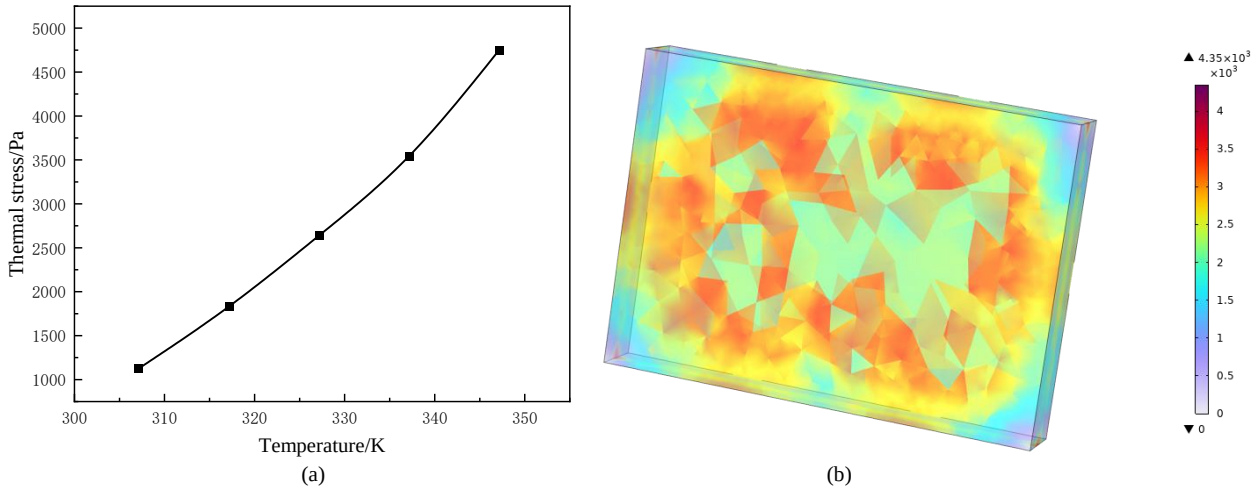

(a) (b)

Fig. 7. Power lithium battery thermal stress distribution law: (a) Thermal stress of lithium power battery at different temperatures; (b) Power lithium battery thermal stress distribution cloud diagram.

attributed to the inertia between the vehicles. The impact surface causes neighboring vehicles to be involved in the impact. In the single-vehicle-to-multi-vehicle and multi-vehicle-to-single-vehicle impact modes, the wagons farther away from the point of impact experience a smaller impact force. Consequently, the hook force on these wagons is also smaller, and the goods in these wagons are subjected to a lesser impact. Thus, the shunting operation scheme also has a substantial impact on the forces acting on the goods. In summary, in the single-vehicle-to-multi-vehicle or multi-vehicle-to-single-vehicle impact modes, efforts should be made to avoid placing power lithium-battery goods in the wagons that are the colliding vehicles.

C. Thermal stress distribution law at different temperatures

This subsection investigates the distribution pattern of thermal stress in the packaging components of lithium-power batteries under different temperature conditions. Fig. 7(a) depicts the thermal-stress curve of the lithium battery at various temperatures. It can be observed from this figure that as the temperature rises, the thermal stress also increases. Fig. 7(b) shows the thermal-stress distribution of the lithium- battery packages after being subjected to a certain temperature for 3600 seconds at an external temperature of 73.2°C. The figure reveals that the thermal-stress distribution of the lithium battery generally decreases from the exterior to the interior, with the lowest thermal stress at the top corner. The maximum thermal stress is found at the points of contact with the six cushioning rubber pads. The minimum thermal stress occurs elsewhere, and the maximum thermal stress is at the contact points with the six cushioning rubber pads. This is because the lithium-power battery expands due to heat, but the cushioning rubber pads restrict its deformation. At these positions, the energy cannot be dissipated through deformation, so the stress is greater. However, the shock absorption provided by the rubber cushions during a collision is far more significant than their effect on thermal stress. Therefore, the packaging design is considered reasonable. Secondly, the temperature difference of the battery cells is $\Delta T_y > \Delta T_x > \Delta T_z$. This temperature difference is derived from Eqs. (5) and (6). The fact that the thermal conductivity along the y-direction is lower than that along the x-direction and the z-direction leads to a relatively larger temperature difference. This implies that heat transfer is more restricted in the y-direction compared to the other two directions, causing uneven temperature distribution within the cells and thus resulting in the observed temperature difference.

D. Stress distribution law of iron box packaging parts

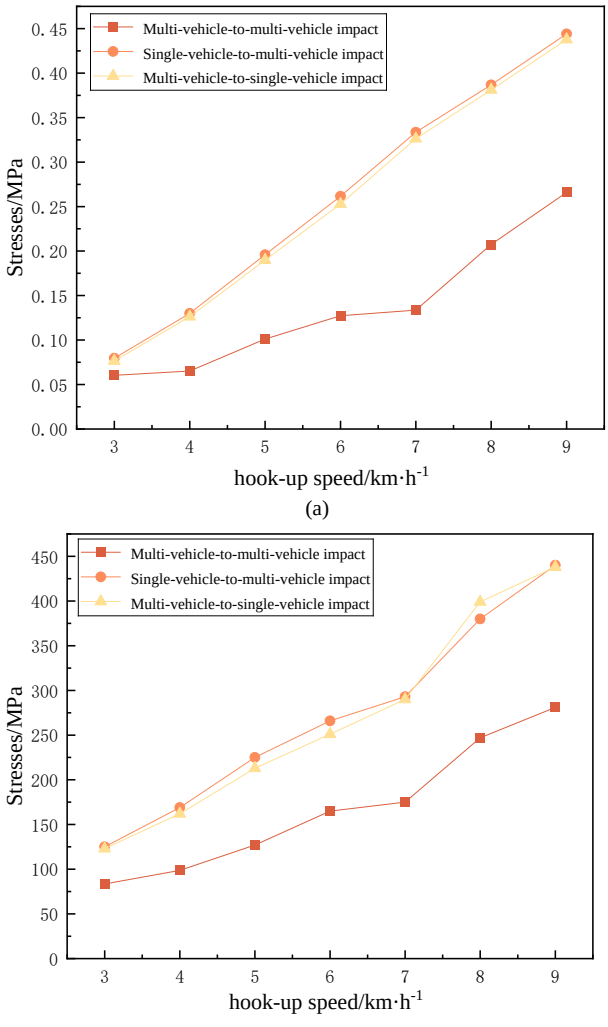

(a)

(b)

Fig. 8. Maximum stresses on steel box packaging subjected to collision in different impact modes: (a) Maximum stress on the battery during a collision; (b) Maximum stress on the outer packaging during collision

This subsection examines the maximum stresses on the outer packaging of lithium-battery packages enclosed in iron boxes under different impact modes, as presented in Fig. 8(b). The maximum value is observed at the rigid connection between the packaging and the container. In the single-vehicle-to-multi-vehicle and multi-vehicle-to-single-vehicle impact modes, when the connection speed is 8 km/h or higher, the maximum stress exceeds the maximum allowable stress of 350 MPa for the outer shell, leading to damage to the outer packaging. However, regarding the maximum stress on the battery itself, as depicted in Figure 8(a), which is the sum of mechanical strain and thermal strain, the maximum stress occurs in the single-vehicle -to-multi-vehicle impact mode. Under the connection condition at a speed of 9 km/h, the maximum stress is 0.444 MPa, which is far less than the allowable stress on the shell of the lithium-power battery, thus meeting the packaging requirements. In addition, when considering the specific internal structure of the battery, the value is still lower than the yield strength of the cell, the PCB board, and the battery cooling plate. As a result, there will be no internal damage to the power lithium-ion battery during the impact process. This indicates that during a collision, the impact energy is absorbed by the buffer material. As a result, the stress transferred to the product is reduced. Since the outer packaging is rigidly connected, it bears a greater impact. At the start of a power lithium-battery cargo collision, the stress gradually increases and reaches its maximum value at 0.12 s. Subsequently, the stress gradually decreases. This is because the collision energy acting on the packaging components is first transferred to the box, then from the box to the cushioning rubber, and finally from the cushioning rubber to the power lithium-battery packages.

Furthermore, to ascertain the critical speed at which the iron box undergoes buckling deformation, a third-degree polynomial fitting approach is employed. This method is used to fit the data corresponding to three distinct collision modes. Through this process, the relationship between the stress value borne by the outer packaging iron box and the connection speed is derived. The fitting equations are presented in sequence as Eqs. (18), (20), and (22), The fitted graph, as indicated, is presented in Fig.9.

$$y_1 = 0.0333x^3 + 2.4536x^2 + 0.1917x + 59.2786 \quad (18)$$

$$R^2 = 0.9833 \quad (19)$$

$$y_2 = x^3 - 15.5357x^2 + 122.6786x - 131.5 \quad (20)$$

$$R^2 = 0.9931 \quad (21)$$

$$y_3 = 0.0278x^3 + 2.9762x^2 + 14.5198x + 53.833 \quad (22)$$

$$R^2 = 0.9857 \quad (23)$$

In the formulas, y_1 , y_2 and y_3 represent the stress values of the outer packaging iron box under different connection speeds in the multi-vehicle-to-multi-vehicle impact mode, single-vehicle-to-multi-vehicle impact mode, and multi- vehicle-to-single-vehicle impact mode respectively. And x is the connection speed of the vehicle, with the unit of km/h. The correlation coefficients of the variables in the formulas are 0.9833,0.9931 and 0.9857 respectively. These high correlation coefficients indicate a very strong correlation between the variables and a good fitting effect of the polynomial models. When the y value (stress value) is set to 350 MPa (the maximum allowable stress of the outer shell), the corresponding x values obtained from the three equations are 10.1695 km/h, 7.7236 km/h, and 7.6264 km/h respectively.

Consequently, in the multi-vehicle-to-multi-vehicle impact mode, the coupling speed should not exceed 10.1695 km/h. In the single-vehicle-to-multi-vehicle impact mode, the coupling speed should not exceed 7.7236 km/h. And in the multi-vehicle-to-single-vehicle impact mode, the coupling speed should not exceed 7.6264 km/h. Exceeding these speeds will lead to damage to the packaging shell, which will not only affect the usability of the packaging but also increase transportation costs.

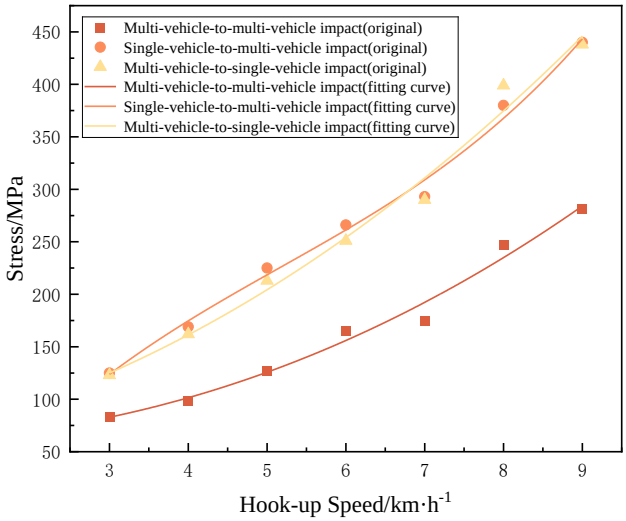

Fig. 9. Data fitting analysis

E. Stress distribution law of corrugated carton packaging parts

In this subsection, the focus is on exploring the maximum stresses on the outer packaging of lithium-battery packages enclosed in corrugated-cardboard boxes under different impact modes, as depicted in Fig. 10(b), and also on the maximum stresses on the batteries themselves, as shown in Fig. 10(a). From the figure, it can be observed that in the single-vehicle-to-multi-vehicle and multi-vehicle-to-single -vehicle impact modes, the forces acting on the packaging components are similar. However, at a coupling speed of 6 km/h, the single-vehicle-to-multi-vehicle impact clearly causes a greater impact. At other coupling speeds, the forces on the packaging components in the single-vehicle-to-multi-vehicle and multi-vehicle-to-single-vehicle impact modes are close to those in the single-vehicle-to-single-vehicle impact mode. Nevertheless, the impact caused by the single-vehicle- to-multi-vehicle impact is still relatively higher. And it can be observed that, under the same collision speed and connection mode, corrugated-cardboard packaging exhibits superior cushioning performance. This is manifested in the fact that both the maximum stress on the outer packaging and the maximum stress on the battery are lower compared to those of iron-box packaging under

identical conditions. The structure of corrugated cardboard allows it to absorb a certain amount of impact energy. It mitigates the external impact force by adjusting its elastic range. On the other hand, an iron box is made of metal material, which has a high degree of rigidity and strength. However, compared to a cardboard box, its elasticity and recoverability are poor. Metal is prone to plastic deformation upon impact and has difficulty returning to its original shape. Consequently, its cushioning performance is inferior to that of a cardboard box. In conclusion, due to its excellent cushioning effect, the cardboard box can provide better protection for the internal products in a dry environment. However, in a humid environment, the increase in humidity will cause the cardboard to soften, the elastic modulus to decrease, and the buffer performance to be reduced[35]. Therefore, in coastal areas, due to the slightly humid climate, the cushioning performance of corrugated boxes will be reduced compared to arid areas. In summary, the plane-shunting operation in the railway transportation of power lithium-batteries is a complex process. It is influenced by multiple factors, including the grouping scheme, collision speed, packaging conditions, humidness and temperature. Therefore, these factors should be considered comprehensively during the operation.

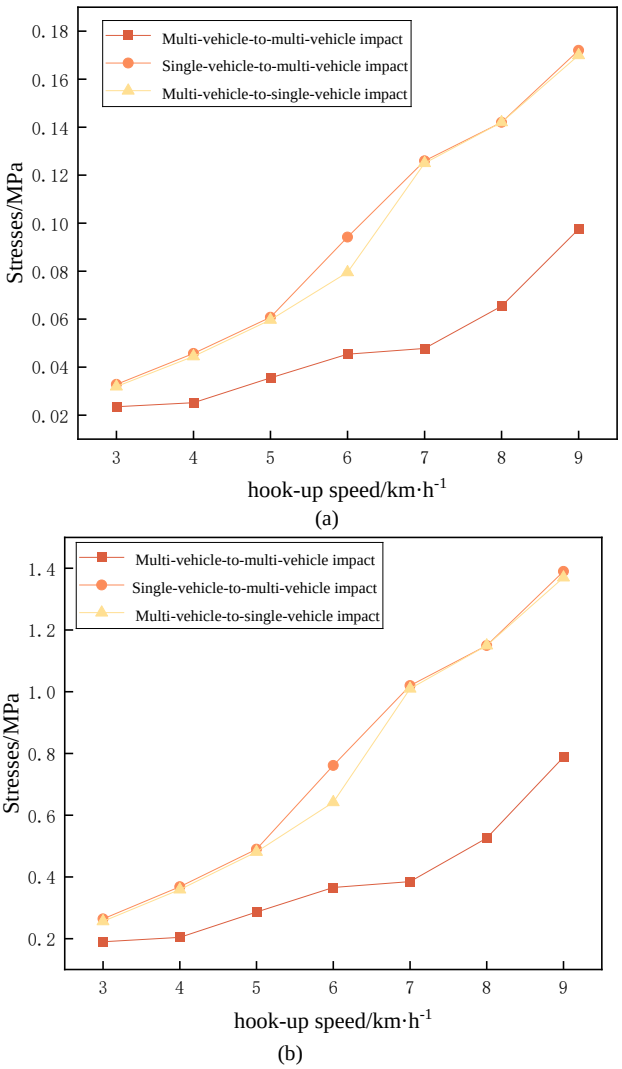

Fig. 10. Maximum stresses on corrugated carton packages subjected to collision in different impact modes: (a) Maximum stress on the battery during a collision; (b) Maximum stress on the outer packaging during collision

V. Conclusion

Considering the influence of temperature on stress, a heat-force coupling model for lithium-power batteries under vehicle-linkage conditions is established. Taking the CATL 1P7S lithium-power battery as an example, two loading and reinforcement schemes, namely iron-box packaging and corrugated-box packaging, are respectively investigated. The impacts of the impact mode, shunting operation scheme, temperature, and loading mode on the stress of the lithium-battery cargo during the vehicle-linkage process are analyzed.

The results indicate that during the railroad-transportation plane-shunting operation, in the multi-vehicle-to-multi-vehicle impact mode, when the connection speed exceeds 10 km/h; in the single-vehicle-to-multi-vehicle impact mode, when the speed exceeds 7.7 km/h; and in the multi-vehicle-to -single-vehicle impact mode, when the speed exceeds 7.6 km/h, the outer packaging of the iron box will be damaged, while the internal product remains undamaged. By contrast, corrugated-box packaging demonstrates better cushioning performance.

The following research directions can be further explored: (1) Given the complex structure of the internal power lithium-battery pack, a more detailed model of the power lithium-battery pack should be established to make the simulation results more consistent with the actual situation. (2) The forces under working conditions such as hump slipping, ascending ramps, and other more complex scenarios still need to be further considered.

References

[1] N. N. Liu, X. C. Zhang, S. J. Dong, et al, “Mechanical response of square lithium-ion battery under different compression loadings,” *Chinese Journal of Applied Mechanics*, vol. 41, no. 04, pp. 797-803, 2024.

[2] Q. Yuan, X. Xu, L. Zhu, et al, “Effects of local thermal accumulation conditions on the thermal characteristics of lithium-ion batteries under high-rate charging,” *Journal of Energy Engineering*, vol. 146, no. 6, pp. 04020072, 2020.

[3] X. Zhang, T. Zhang, N. Liu, et al, “Dynamic crushing behaviors and failure of cylindrical lithium-ion batteries subjected to impact loading,” *Engineering Failure Analysis*, 2023, 154: 107653.

[4] S. W. Y. XU, P. L. HE, X. D. WANG, et al, “Applicability Research on UN38.3 for Railroad Transport of Lithium Battery,” *China Standardization*, no. 15, pp. 238-242, 2021.

[5] Mukhopadhyay A, Sheldon B W, “Deformation and stress in electrode materials for Li-ion batteries,” *Progress in Materials Science*, no. 63, pp. 58-116, 2014.

[6] S. C. Chen, C. C. Wan, Y. Y. Wang, “Thermal analysis of lithium-ion batteries,” *Journal of Power Sources*, vol. 140.no. 1, pp. 111-124, 2005.

[7] P. Nie, S. W. Zhang, A. Ran, et al, “Full-cycle electrochemical-thermal coupling analysis for commercial lithium-ion batteries,” *Applied Thermal Engineering*, vol. 184, pp. 116258, 2021.

[8] Y. Suo, J. Liu, “Thermo - mechanical coupling analysis of a cylindrical lithium - ion battery with thermal radiation effect in generalized plane strain condition,” *International Journal of Energy Research*, vol. 45, no. 2, pp. 1988-1998, 2021.

[9] Y. Suo, G. Lai, Z. He, “A Fully Coupled Thermomechanical Analysis of Lithium-Ion Batteries with Total Heat Generation Rate,” *Journal of Energy Engineering*, vol. 149, no. 6, pp. 04023042, 2023.

[10] B. Liu, H. Zhao, H. Yu, et al, “Multiphysics computational framework for cylindrical lithium-ion batteries under mechanical abusive loading,” *Electrochimica Acta*, vol. 256, pp. 172-184, 2017.

[11] C. Yuan, X. Gao, H. K. Wong, et al, “A multiphysics computational framework for cylindrical battery behavior upon mechanical loading

based on LS-DYNA," *Journal of The Electrochemical Society*, vol. 166, no. 6, pp. A1160, 2019.
[12] D. Kang, P. Y. Lee, K. Yoo, et al, "Internal thermal network model-based inner temperature distribution of high-power lithium-ion battery packs with different shapes for thermal management," *Journal of Energy Storage*, vol. 27, pp. 101017, 2020.
[13] G. F. Gong, X. J. He, J. M. Zhou, et al, "Simulation analysis on fall of a type of lithium battery fully paper-based packaging parts," *Packing Engineering*, vol . 44, no. 13, pp. 277-284, 2023.
[14] Z. Q. Li, Y. Y. Tian, S.Q. Liu, "Transport packaging design and drop simulation analysis of lithium battery," *Packing Engineering*, vol. 43, no. 21, pp. 137-143,2022.
[15] S. X. Huang, H. S. Xu, Q. P. Wang, et al, "Study on The Response Characteristics of Cylindrical Power Lithium-ion Batteries under Impact Load," *Energy Storage Science and Technology*, vol. 10, no. 13, pp. 3642-3652, 2024.
[16] Z Bai, X Zhao, H Song, et al. "Prediction of Back-layering Length and Critical Velocity with Lithium-ion Battery Car Fires in Tunnel," *IAENG International Journal of Applied Mathematics*, vol. 54, no. 6, pp. 1033-1037, 2024.
[17] H Zheng, L Zuo. "Two-grid Domain Decomposition Method for Coupling of Fluid Flow with Porous Media Flow," *IAENG International Journal of Applied Mathematics*, vol. 54, no. 9, pp. 1711-1716 , 2024.
[18] V Keerthika, R Prahalatha. "Series Solution of Non-linear Initial Value Problems on Certain Physical Systems through MATLAB," *IAENG International Journal of Applied Mathematics*, vol. 54, no. 10, pp. 2118-2127, 2024.
[19] L.Z. WANG, "Exploration of various inertial forces acting on goods," *Railway Transport and Economy*, vol. 02, pp. 25-27+29, 1983.
[20] X. D. WU, P. X. BAO, Y. W. YANG, et al, "Research on simulation of military wheel-equipment railway transportation impact test by SIMPACK," *Journal of System Simulation*, vol. 21, no. 16, pp. 5025-5029, 2009.
[21] C. I. Crăciun, M. Dumitriu, "Distribution of Longitudinal Forces in the Body of Passenger Trains," *Applied Mechanics and Materials*, vol. 809, pp. 1175-1180, 2015.
[22] C. Crăciun, C. Cruceanu, "Influence of resistance to motion of railway vehicles on the longitudinal trains dynamics," *MATEC Web of Conferences*. *EDP Sciences*, vol. 178, pp. 06003, 2018.
[23] C. Cruceanu, M. Dumitriu, C. Crăciun, "About the influence of wheel slide protection devices action on longitudinal dynamic of trains," *MATEC Web of Conferences. EDP Sciences*, vol, 112, pp. 07012, 2017.
[24] J. Wang, H. A. Rakha, "Longitudinal train dynamics model for a rail transit simulation system," *Transportation Research Part C: Emerging Technologies*, vol. 86, pp. 111-123, 2018.
[25] X. B. Zhao, "Research on optimization of draft gear characteristics for freight cars," *Dalian Jiaotong University*, 2021.
[26] Z. Fu, "Research on dynamic model of MT-2 draft gear based on impact test," *Dalian Jiaotong University*, 2018.
[27] R. J. Wang, "Research on the longitudinal impact characteristics of railway freight cars and the influence of key draft gear parameters," *Beijing Jiaotong University*, 2021.
[28] K. Y. Zeng, X. Y. Hu, J. L. LIU, et al, "Analysis of Coupling Characteristics of the 102-Type Coupler Under Tight Radius Curve Conditions," *Journal of Xihua University (Natural Science Edition)*, (Online), 1-8, Available: https://link.cnki.net/urlid/51. 1686.n. 20240130.1551.002.
[29] C. Y. Chang, Y. M. Ma, G. Guo, et al, "Simulation study on the influence law of longitudinal force on ultra-long and heavy-duty trains," *China Railway Science*, vol. 42, no. 01, pp. 87-94, 2021.
[30] D. Q. Wen, F. Wang, J. Shi, et al, "Safety analysis of train operation in long downhill curve sections of heavy haul railways," *China Safety Science Journal*, vol. 32, no. 06, pp. 87-94,2022.
[31] Y. Z. Peng "Study on mechanism and simulation experiment of the influences of railroad wagon loading conditions on vehicle running safety," *Beijing Jiaotong University*, 2013.
[32] S. Y. Zhao, R. L. Tian, C. G. Wang, et al, "Research on environment conditions of temperature and humidity inside container in southeast coast region," *Equipment Environment Engineering*, no. 01, pp. 44-47, 2007.
[33] W Mei, H Chen, J Sun, et al. "Numerical study on tab dimension optimization of lithium-ion battery from the thermal safety perspective", *Applied Thermal Engineering*, no. 142, pp. 148-165, 2018.
[34] G.N. Ellison, Thermal Computations for Electronic Equipment, VanNostrand Reinhold, New York, 1969.
[35] S Sun, J Wang. "Influence of Humidity on Corrugated Board's Longitudinal Compression Bearing Performance", *Packing Engineering*, vol. 42, no. 19, pp. 178-184, 2021.